

Thesis for the degree of Licentiate of Technology
Sundsvall 2017

Measuring Water Droplets to Detect Atmospheric Icing

Staffan Rydblom

Supervisor: Associate Professor Benny Thörnberg,
Professor Mattias O'Nils

Department of Electronics Design, in the
Faculty of Science, Technology and Media
Mid Sweden University, SE-851 70 Sundsvall, Sweden

ISSN XXXX-XXXX

ISBN XXXX-XXXX

Mid Sweden University Licentiate Thesis XX



Akademisk avhandling som med tillstånd av Mittuniversitetet i Sundsvall framläggs till offentlig för avläggande av licentiatexamen i elektronik **måndagen den 28 Augusti 2017**, klockan **13.00** i sal **M102**, Mittuniversitetet Sundsvall. Seminariet kommer att hållas på engelska.

Measuring Water Droplets to Detect Atmospheric Icing

Staffan Rydbom

©Staffan Rydbom, 2017

Electronics Design Division, in the Faculty of Science, Technology and Media Mid Sweden University, SE-851 70 Sundsvall Sweden

Telephone: +46 (0)60 148422

Printed by Kopieringen Mittuniversitetet, Sundsvall, Sweden, 2017

This is dedicated to...

ABSTRACT

This thesis is about...

SAMMANFATTNING

Den här avhandlingen handlar om...

CONTENTS

LIST OF FIGURES

LIST OF TABLES

LIST OF PAPERS

This thesis is based on the following papers, herein referred to by their Roman numerals:

PAPER I

- Liquid Water Content and Droplet Sizing Shadowgraph Measuring System for Wind Turbine Icing Detection
S.Rydbom, B. Thörnberg, IEEE Sensors Journal, 2015 ??

PAPER II

- Droplet Imaging Instrument - Metrology Instrument for Icing Condition Detection
S.Rydbom, B. Thörnberg, IEEE International Conference on Imaging Systems and Techniques (IST) Proceedings, 2016 .. ??

PAPER III

- Liquid Water Content and Droplet Sizing Shadowgraph Measuring System for Wind Turbine Icing Detection
S.Rydbom, B. Thörnberg, Measurement Science and Technology, 2017 ??

PAPER IV

- Field Study of Ground-LWC using the Droplet Imaging Instrument
S.Rydbom, B. Thörnberg, P. Jonsson, E. Olsson, Cold Regions Science and Technology, 2017 ??

— Chapter 1 —

INTRODUCTION

This thesis is am exploration of a method to measure the size and concentration of atmospheric liquid water, with the purpose of finding a cost efficient technique to detect the conditions for icing on structures.

The measurement method is based on digital image processing of a shadowgraph system using LED light as background illumination. The instrument is constructed using standard components with the intent of viewing possibilities of low cost volume production. It may e.g. be used for real-time icing condition measurement, or remote meteorological data collection.

Paper I describes a shadowgraph system that uses edge detection to define a measurement range depending on the size of a particle and the image signal to noise ratio (SNR). Paper II describes the design of a weather protected prototype and a fog chamber used for initial tests. Paper III is a verification of the size measurement using polymer microspheres in calibrated (NIST traceable) distributions. Paper IV is an field study of ground LWC and MVD using the DII and a comparative study using the CDP.

1.1 Atmospheric Water and Icing

Measuring and controlling the properties of a fog of water droplets has been the interest and focus of many studies during at least half a century. Applications range from atmospheric studies, aircraft safety to military and commercial applications.

Icing caused by freezing atmospheric water can be a significant problem in cold climates, affecting infrastructure such as wind turbines, power lines, and road and air traffic. With the increasing importance of electric power generated by wind, there is a renewed demand predictions of icing on wind turbines. Icing on the blades of a turbine lowers the efficiency, increases noise and may force the turbine to a complete stop [11, 15, 23, 25]. Aircraft, power lines or any other weather exposed structure share this problem. Therefore big efforts have been made to create models for how the ice is formed [35,

36, 45] and how it can be included in weather prediction models [48, 30].

1.2 Related Work of Measurement

In 1970, Knollenberg [26] described an electro-optical technique to measure cloud and precipitation particles using a laser illuminated linear array of photo detectors. The photo detectors are used to make a two-dimensional image of the particles' shadows as they pass the light beam. Systems based on this technique are called Optical Array Probes (OAP) or two-dimensional imaging probes. Developments of this technique include using image sensors to save gray scale images of the detected particles [32, 52]. The Droplet Imaging Instrument (DII) developed and described in this thesis is based on this technique.

Light scattered from a focused laser [3, 12] is a different technique to measure single particles. A laser beam is used to illuminate passing particles. When a particle is detected, its size is determined by comparing the variations in light with a pattern derived from the Mie scattering solutions [38]. The Cloud Droplet Probe (CDP) used as a reference instrument is based on this technique.

The OAP, imaging and the light scattering spectrometers each have some advantages over the other technique depending on the nature of the aerosol. Instruments for airborne use have been developed that combine several techniques into one single probe for accurate measuring of LWC and MVD [5, 4].

A similar but different optical technique for measuring water droplets is based on in line holography [33]. In principle this is a two-dimensional shadowgraph imaging system that use laser background illumination to create images of the diffraction patterns created by the passing particles. These patterns are measured to reconstruct images of the particles. This is a fairly calculation intensive process, which may be one of the reasons why instruments based on this technique are not so common yet [20]. An advantage with this technique is the increased measurement range, i.e. the useable depth in each image.

Sizing of the droplets using Mie spectrometry is a complex operation even for coherent light citebohr2008, and although it is possible to study Mie scattering from white light [51], the complexity, small

1.2. Related Work of Measurement

droplet size range and sample volume makes it less attractive in this application. The optical resolution is usually too low. Therefore it is also difficult to determine the exact particle size and the usable depth of field for incoherent shadowgraph systems. The shadow from a particle can e.g. appear smaller or larger when out of focus.

Shadowgraph imaging of particles using incoherent illumination instead of laser has been tried e.g. in particle shadow velocimetry (PSV) [13], or spray characterization [54]. Quantitative and comprehensive studies of other droplet measurement techniques exist [12, 20, 10].

Kuhn et. al. [31] described a method to characterize ice particles by Fourier shape descriptors [18, 50]. The system uses a microscope-like technique to achieve a high resolution level, in the order of one micrometer. Although not specifically designed to measure water droplets, the principal design is similar to the DII. It has a field of view of 200x150um and a depth of field of approximately ten micrometers.

— Chapter 2 —

THEORY

In this chapter the first section introduce the physics behind the forming of ice on structures. The next two sections is briefly describing the measurement parameters and some practical problems of measuring icing. The last section is about scattering of light by small particles.

2.1 Forming of Ice

The icing process is complex and the result depends on a combination of the aerodynamic shape of the structure or airfoil, the velocity of the air and its contained water, the temperature, the mixing of snow and water, the concentration of liquid water and the droplet size distribution. The figure below illustrates the difference between large and small supercooled droplets passing an aerodynamic profile.

A particle's eagerness to follow the flow or collide depends on several factors, like the flow velocity, the size of the obstacle, the density and drag coefficient of the particle. This relationship is known in fluid mechanics as the Stokes number (Stk). Small droplets or particles with $Stk \ll 1$ may continue with the airflow around the profile, while large droplets or particles with $Stk \gg 1$ due to their

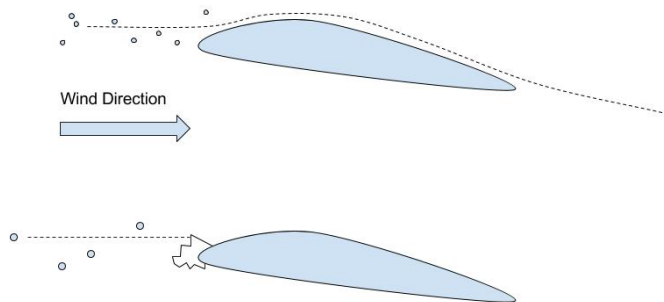


Figure 2.1: Supercooled water droplets on collision course with an aerodynamic profile.

inertia collide with the structure. A supercooled droplet colliding with a structure would likely freeze on the impact.

Icing on wind turbines forms slightly differently from the ice accretion on an aircraft airfoil. Since the turbine is stationary it cannot stop the icing, or de-ice by moving to a different position. The same conditions may persist for days or weeks. The turbine blade moves concentrically making the tip of the blade the fastest, and highest located moving part. There is no pilot or ground crew supervising the wings. Therefore the remote and exposed position makes it difficult to detect ice directly when it is initially formed [21].

Add picture
of ice on
top of wind-
turbine

2.2 Liquid Water Content and Median Volume Diameter

The liquid water content (LWC) and the water droplets median volume diameter (MVD) are parameters that can be used to predict or model icing. The MVD is given at the point where half of the total volume of liquid content in a fixed air volume consists of droplets with diameters larger and the other half has smaller diameters. To estimate the amount of icing created by supercooled water droplets, for most cases the MVD has been shown to be a good indicator [34, 16].

In practice, the LWC and the MVD are scarcely ever measured at a planned or existing wind turbine [41, 34]. Measuring these properties accurately and frequently would be an advantage for the planning of new wind mill farms or for the application of anti-icing arrangements on existing power stations. It may be of particular interest as input to weather prediction models by which both LWC and MVD can be computed [48, 39]. In combination with information about the aerodynamic properties of the wind turbine, it can give more accurate predictions of icing or even result in better design of wind turbines and anti-icing methods.

While icing caused by large supercooled droplets, with diameters from approximately 50 μm to exceeding 1000 μm , is often considered severe due to its shape and quick build-up, icing may occur even with droplets as small as 5 μm [44, 8, 22]. In most cases, though, icing is caused by cloud droplets measuring between 10 μm and 30 μm in diameter [34, 8]. Although optical imaging and other techniques for measuring aerosol properties is continuously improving, the choice of

2.3. Practical Problems with Measuring LWC, MVD and Ice

instrument is still very much dependent on the application's requirements [24, 3, 4, 32]. An instrument for measuring icing parameters for wind turbines should be able to detect supercooled cloud droplets from five micrometer and determine an accurate measure of the LWC. Since measurements are needed in multiple remote locations it should also be affordable, reliable, have low power consumption, and ideally be possible to place near the highest point of the turbine [21].

2.3 Practical Problems with Measuring LWC, MVD and Ice

Many existing instruments suffer from errors caused by the instrument itself during sampling, e.g. when droplets get stuck on the inlet [46]. At higher wind speeds particles shatter into smaller droplets or bounce on the supporting structure making up the instrument [9, 14]. All droplets or particles approaching an obstacle are affected by the change in pressure and wind direction surrounding it, a fact which complicates measuring the concentration of particles in unaffected air. Measurement probes working by extraction of air using a mechanical air pump would expect a loss of particles with large Stokes numbers. Ideally the measuring device should be designed in order to affect the free flow of particles as little as possible [4].

Some instruments on the other hand use the fact that supercooled water droplets will freeze on the impact, e.g. the rotating cylinders used by Makkonen [34]. By exposing cylinders of different diameter for passing stream, the MVD and LWC can be calculated depending on the amount of ice accumulated on each cylinder. While this technique provides a nice alternative to the single particle measurements its drawback is that it requires some manual operation and of course the fact that only freezing water can be measured.

Measuring particles from aircraft is partly made complicated by the high air speed. The sample is affected by the change in pressure surrounding the aircraft and by particles hitting parts of the probe, splintering or changing direction. (ref) An instrument fixed to the ground on the other hand is affected by the wind speed relative to the ground. This means that it needs to be directed in the direction of the wind. Particles may also enter the measurement zone from different

Chapter 2. Theory

directions depending on their Stokes number, which has been shown to have an effect on the measured liquid water content [20].

Another difficulty regarding the measurement of hydrometeorors in general is the large size differences ranging from micrometer-sized fog droplets or graupel to raindrops several mm in diameter, even larger snowflakes or ice hail. Since the water content and the resulting icing depends on all these categories each or of combinations, several different instruments are usually needed to cover the whole range of sizes and nature of particles. An imaging instrument is limited by the optical system's resolution, it's field of view and the usable depth of field, which we have called the measurement range.

Instruments based on Mie calculations of light scattering have the issue of dealing with the non-linear relation between scattering response and diameter. Aliasing in the sample bin resolution can lead to spikes in the size distribution. Two particles with different diameter, particularly interesting in the 10 to 15 μm range, can even have the same scattering intensity response [12, 46, 6].

2.4 Light Spectrum

In visible light, water is almost transparent. This means that the imaginary part of the refractive index, i.e. the absorption, is very small, while for some higher and lower wavelengths it increases with a factor of almost ten power to ten [29]. This fact is used in two-color lidar measurements [53]. The real part of the refractive index for water is much more stable, approximately 1.34 at 455 nm light [19]. For simplicity we have assumed that the refractive index of air is equal to one.

A droplet works as a spherical lens with a very short focal length. Exposed to a background illumination it will scatter almost all of the light reaches the droplet in different directions, causing a shadow that appears as a black disc except for the refracted light passing straight through the center. Some of the light will of course be absorbed, albeit the absorption of a single water droplet is negligible due to its small volume and because water absorb very little in the visible spectrum.

When the light source is spread out compared with the size of the droplets, as in the case of using a collimated LED, the intensity of the

2.4. Light Spectrum

center Arago spot caused by Fresnel diffraction would be negligible [42].

The combined effect of scattering and absorption is the extinction [6]. Due to this combined effect, clouds look nontransparent from a distance. Measuring extinction is possible in aerosols e.g. by using Raman LIDAR [2].

MATERIALS AND METHODS

The work begun with some initial tests, where we experimented using different light sources and illumination angles. We then decided to continue using a shadowgraph system with background illumination. The experimental setup was tested using different water droplet generators and a test target consisting of micrometer sized lines and dots. Analyzing the optical system and testing different segmentation algorithms we found a simple way to define the sample volume from a single image. Using the Laplacian of Gaussian edge detection, which principally is a second derivation of the image intensity gradient, and a suitable threshold, we can create closed curves around objects where the edge is in or near focus. To test the ability of measuring concentration we needed to build a weather protected prototype that could be used in parallel with a second instrument. The prototype needed to be fully automatic, able to analyze images in real time 24 hours a day during several months and store the results in a compressed format. To calibrate the size measurement and the measurement range, the previously mentioned dots of different sizes were used. The size measurement was also verified using distributions polymer microspheres, applied by blowing compressed air through a glass dispenser.

3.1 Image Segmentation

Edge detection can be done in several ways. The simplest method is to use a threshold at a fixed level and define the edge as the transition between above and below that threshold [17]. Other techniques use different methods to measure the gradient of the change in intensity [7, 37].

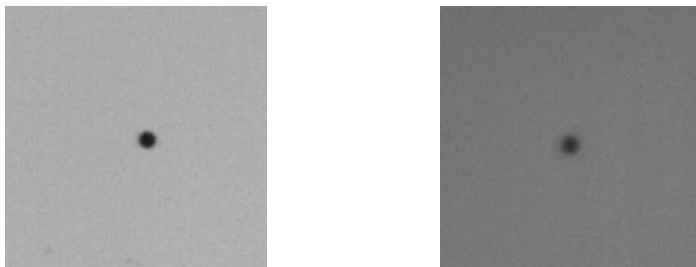


Figure 3.1: Same dot viewed in different background light. 455 nm (left) and 850 nm (right).

3.2 Starting Studies

We describe the measured droplets as spherical lenses made of pure water at a constant temperature, surrounded by air.

3.2.1 *Light Spectrum*

Although water is a good absorber of electromagnetic radiation in most spectral wavelengths except for the visible, the volume of water droplets is too small for the absorption to be measurable. In visible light, the water droplet can be regarded as a spherical lens with a very short focal length, thus spreading most of the light in diverging directions. Since the used camera is specifically designed for visible and near infrared, we tested and compared two different wavelengths, 455 nm and 850 nm using the same optical setup. The shorter wavelength gave sharper images.

One would expect diffraction patterns depending on the spectral bandwidth of the light source. The narrower band width the stronger the diffraction would be. A spectrum analyze of the LED showed that the coherence length of the blue LED is about 6.8 μm .

3.2.2. Laser Light

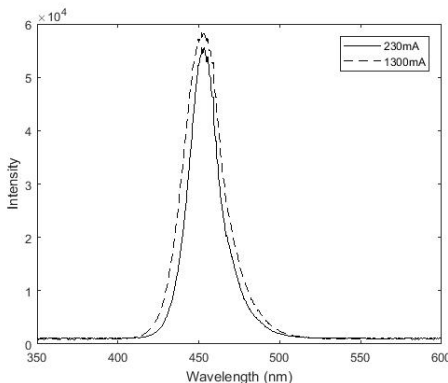


Figure 3.2: Spectrum of the Mightex 455nm LED using two different driving currents. The band width is slightly wider for the higher current.

3.2.2 *Laser Light*

3.2.3 *Image Noise*

3.2.4 *Light Sensitivity Measurement*

3.2.5 *Speed of Light Flash*

A value of both MVD and LWC can be derived from a series of images and since the number of measured droplets will depend on the concentration, the accuracy and precision will depend on the number of samples from the total population of droplets.

We also investigate the illuminative power required to get a good exposure with the tested system at a targeted maximum wind speed of 50 m/s.

3.3 Design Considerations

3.4 Dot Reference Measurement

The dots on the micrometer scale were measured visually using a Leica microscope connected to a digital camera. This was done to get

Chapter 3. Materials and Methods

accurate values of the diameter of the dots for use in the calibration. An example image that was measured can be seen in ??.

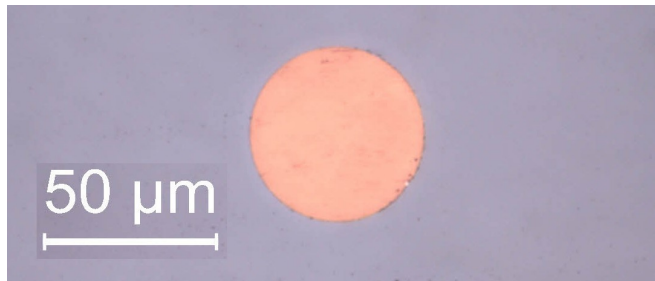


Figure 3.3: The 50 micrometer dot with front illumination imaged using 40x magnifying lens.

This measurement was done using lenses with two different magnifications: 40x and 100x. All the dots average diameters, except the 100 μm dot were found to be within $+/-0.2 \mu\text{m}$ of their nominal diameter. They are not all perfectly round, but the size accuracy should be good enough to use as calibration reference. The result from this measurement is comprehended in ??.

Nominal Diameter	Excentricity	Diam. 40x	Diam. 100x
5	0.2	5	4.8
6	0.6	5.8	5.8
7	0	7	6.6
8	0	8	7.9
9	0	9	8.8
10	0	10.1	9.8
25	0	24.9	24.7
50	0.4	50.1	49.8
75	0.2	75.2	74.8
100	2.5	100	98.7

Table 3.1: Micro dot verification measurement. All values are in μm . b. Eccentricity is here the maximum difference between the smallest and the largest measured diameter.

3.5 The Shadowgraph System

The instrument is a shadowgraph system using a monochrome CMOS camera with a 4x magnifying telecentric lens and a LED with a collimating lens illuminating the background. The blue LED is powered by a current driver able to produce short 12 A current pulses. Figure ?? shows a sketch of the system.

The system is mounted in a weather proof shell using two standard camera housings and a separate box for the analyzing computer and power supply. Fig. 2 shows the system mounted in weather proof camera housings.

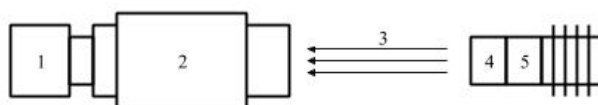


Figure 3.4: Principle of shadowgraphy. 1. Camera. 2. Telecentric lens. 3. Parallel focused light beam. 4. Collimating lens. 5. LED.

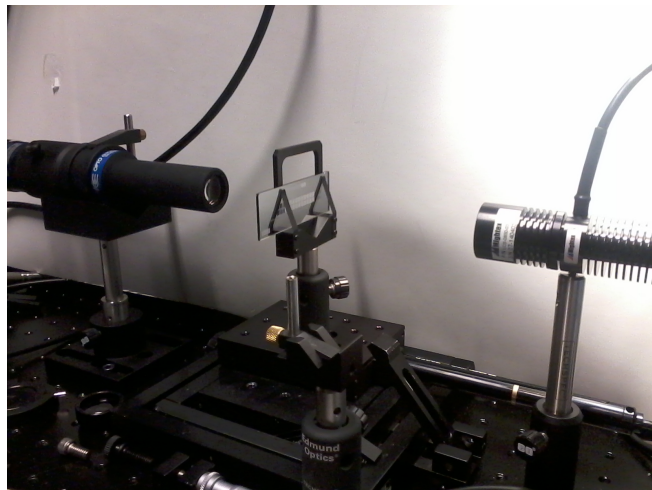


Figure 3.5: The experimental setup with a dot micrometer scale as test object mounted on a translation stage.



Figure 3.6: The illumination and detector is mounted inside two Bosch camera housings facing each other with heating inside the house and on the front glass.

Calibration of true droplet size and measuring range both depends on the measured size of the droplet shadow and the amount of light used for exposure. It is possible to predict both the precision of the measured size and accuracy for measurement of droplet size.

We used a stage micrometer scale for characterization of the system and simulation of water droplets. This characterization holds true given that the optical silhouette of a droplet is comparable to a dot having equal diameter and being printed on a silicon glass. It is not a new concept and has at least once been proved experimentally, by comparing with beads of glass and water droplets of known sizes [28, 27]. The shadow image of water drops of any size will be defined mainly by the diffracted component, as long as the distance between the drop and the lens is much larger than the drop diameter [28, 52].

The design using a weakly collimated LED that illuminates an area slightly larger than the field of view makes the system quite insensitive to misalignment of the camera and the light source. Temporal or permanent changes in light intensity caused by a minor misalignment is automatically compensated for by continuous measurement of the total exposure level. If the level of exposure is increasing or decreasing, the length of the light pulse is changed correspondingly. The light intensity can also be affected by dirt on the front glass of the housings.

Since many images will not contain any droplet at all, we can increase the processing speed by sorting out the images that are not

3.5.1. Exposure Check and Flash Intensity Adjustment

containing any interesting information. This is done by constructing an average image from 20 images and use this as a flat-field correction. All new images are compared with this average and if any pixel differs from the average by more than a specific value that is significantly higher than the noise level, the image is analyzed.

Spatial dissimilarities in the light intensity that are not caused by noise are compensated for by calculating the local average intensity of the background around each measured droplet. The size of a droplet is then based on the intensity dip caused by the shadow compared with its local background.

3.5.1 *Exposure Check and Flash Intensity Adjustment*

Let $I_{i,j}$ depict the two dimensional image captured by the camera. The mean value \bar{i} of all pixels in the image $I_{i,j}$ gives an estimation of the exposure level in the whole image.

The flash duration is adjusted automatically by the microcontroller at each exposure to keep the exposure level between a low and a high threshold, th_L and th_H . The duration is changed in steps of 13 ns corresponding to one clock cycle of the microcontroller. If $\bar{i} > th_L$ and $\bar{i} < th_H$ the image is analyzed. If $\bar{i} \geq th_H$ the flash duration is decreased by steps of 12 ns. If $\bar{i} \leq th_L$ the flash duration is increased. The total flash duration is approximately 250 ns. th_L is here set to 0.7 and th_H is set to 0.8 in a normalized (0,1) dynamic range.

3.5.2 *Edge Detection and Edge Sharpness*

To detect the intensity changes created by the shadow of a water droplet, an image is processed using the from edge detection theory well known Laplacian of Gaussian (LoG) described by Marr and Hildreth [37]. The method works by looking for zero crossings in the image resulting from calculating $\nabla^2 G(x, y) * I(x, y)$. $G(x, y)$ is a two dimensional Gaussian distribution with standard deviation σ and ∇^2 is the Laplacian operator, defined as the divergence of the gradient in two dimensions.

$$G(x, y) = \frac{1}{\pi\sigma^2} e^{-\frac{x^2+y^2}{2\sigma^2}} \quad (3.1)$$

Chapter 3. Materials and Methods

$$\nabla^2 = \nabla \cdot \nabla = \frac{\delta^2}{\delta x^2} + \frac{\delta^2}{\delta y^2} \quad (3.2)$$

We implement a discrete approximation to $\nabla^2 G(x, y) \approx \nabla^2 G_{i,j}$ as a 13x13 sized convolution kernel.

$$\nabla^2 G_{i,j} = -\frac{1}{\pi\sigma^4} \left(1 - \frac{i^2 + j^2}{2\sigma^2}\right) e^{-\frac{i^2+j^2}{2\sigma^2}} \quad (3.3)$$

By applying the convolution to the normalized image $I_{i,j}$ we get the resulting image $P_{i,j}$.

$$P_{i,j} = \nabla^2 G_{i,j} * I_{i,j} \quad (3.4)$$

$P_{i,j}$ is thus a matrix that contains the second order derivative of the image $I_{i,j}$. A spherical object will cause an edge where the intensity change is similar around a spherical object, but dependent on the distance from the optimal focus. Assuming the Gaussian of the image I is twice differentiable at any point (i, j) , the maximum (or minimum) of the second derivative includes the amplitude of the first derivative at the point where the second derivative is equal to zero, i.e. where the edge is strongest. This can be intuitively understood when considering that if the edge is sharper, the gradient, or first derivative value is larger, and if the gradient value is larger the rate of change, i.e. the second derivative needs to be larger at each side of the edge. Therefore we store a value of the maximum second derivative, $\max(P_{i,j})$, around each analyzed object and use this as a measure of the edge sharpness. This value is then used as input to a calibration function. We also construct a new binary image Q in which the pixel value $Q_{i,j} = 1$ if any of $|P_{i+1,j} - P_{i,j}|, |P_{i-1,j} - P_{i,j}|, |P_{i,j+1} - P_{i,j}|, |P_{i,j-1} - P_{i,j}| > th$, where $th = 0.002$. $Q_{i,j} = 0$ elsewhere. th is the gradient of the second derivative at the point where the second derivative is zero, i.e. on the edge. Particles are found by searching for closed contours in this binary image.

3.5.3 Comparing Transparent Microspheres and Dots

A spherical lens scatters almost all the incident light in different directions, leaving only a bright spot in the middle where light is transferred directly through. For larger particles in focus, this bright

3.5.4. Removing the Center Bright Spot

spot will result in a second circular closed contour inside the outer edge.

Small water droplets can be seen as transparent microspheres. The composition changes the refractive index, but this has little effect on the shadow. The outer contour is the same following the same reasoning as with the dots used for calibration [43]. Diffraction patterns depend on the wavelength of the light and the size of the sphere. The resolution of the constructed system is not high enough for these patterns to be visible.

By using a flood-fill function on the binary image containing the detected contour, starting in a point at a minimum distance from an object, the edge of the filled area will border to the outer contour. This makes it possible to select the outer closed contours of possible particles.

3.5.4 Removing the Center Bright Spot

The center bright spot will make the shadow of a transparent sphere brighter in average than a solid dot. This will have an impact on the size calculation, since the size calculation is based on the shadow impact and the calibration is done using solid dots. Therefore we apply a mask on the image before calculating the size of the shadow. The mask is done by replacing all the centermost pixels in a shape of a circular disc with the intensity of the darkest pixel in the spot. The diameter of the masked disc is the arc length of the edge contour divided by 4π . The bright spot is measured by calculating the difference between the least value and the center pixel. Only particles with a difference larger than 0.1 (ten percent) will have the mask applied

3.5.5 Measuring Roundness

There may be clogs of small microspheres or dust in the samples that are measured. Microspheres, or small water droplets are close to spherical. Therefore we try to exclude all objects that the program find but are not circular. After the detection of object edges, we measure the roundness of each object. A measure of the mean square roundness deviation similar to the one described by ISO [40] can be achieved by

Chapter 3. Materials and Methods

calculating the quote between the area of the contour and the square of the total arc length See (??).

$$roundness = 4\pi \frac{A_{contour}}{arcLength^2} \quad (3.5)$$

$A_{contour}$ is the pixel area of the contour and $arcLength$ is the perimeter of the measured closed contour. In the calibration and field measurements described, an object is only considered spherical if $roundness \geq 0.85$.

3.6 The Fog Chamber

The fog chamber is needed to create a test environment for the instrument. Natural fogs tend not to occur outside just when we are ready to test. If possible, it is desirable that the environment can be controlled and verified using a second instrument. It gives an indication of how the instrument will behave in a real measurement. It is also a verification of the instrument's water ingress resistance.

The constructed chamber has a frame made of 30 mm aluminum profiles, fitted with transparent 6 mm polycarbonate walls on all sides using rubber sealing strips. The droplets are produced using an ultrasonic fog generator pushing the droplets to the chamber through a flexible tube approximately 30 mm in diameter and 500 mm long. Next to the fog inlet, there is a dry air inlet with a speed adjustable fan. On the back of the chamber there is a similar sized outlet for air and moisture.

3.7 The Klövsjö Installation

Figure ?? shows the installation. On top is the two camera houses of the DII and just below is the smaller CDP. The Lambrecht Eolos weather sensor is seen furthest to the left, mounted on an horizontal boom. In the middle just right of the Eolos is the mobile communication antenna. In the lower center the top of the shortened lattice mast is seen and behind this is the box containing the DII processing computer, the CDP data collection computer and the communications router. The whole installation is about five meters high. An electric

3.7. The Klövsjö Installation

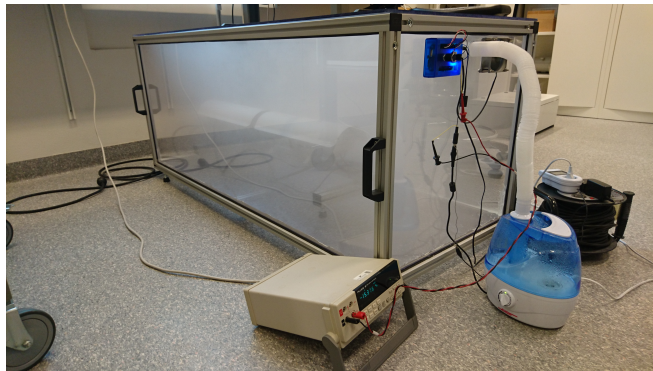


Figure 3.7: Fog chamber with connected droplet generator (blue container) and a multimeter used for fan power measurement. A Beaglebone Black microcontroller (blue box) is used for fan speed regulation.

servomotor mounted at the base of the pole inside the lattice mast rotates the two instruments automatically to follow the horizontal direction of the wind.

?? shows icing on the front side of the installation.



Figure 3.8: Icing on the front side of the installed instruments.

Chapter 3. Materials and Methods



Figure 3.9: Installation in Klövsjö.

— Chapter 4 —

DISCUSSION

4.1 Starting Studies

4.1.1 *Infrared and Visible Light*

4.1.2 *Laser Light*

4.1.3 *Image Noise - SNR*

Light Sensitivity Measurement

4.1.4 *Speed of Light Flash*

The LED used was fully functional after four months of continuous measurements using 12 times higher current than specified. Using even higher current

4.2 Aerodynamics

4.3 Difficulties with Polymer Microspheres

To get a second verification of the sizing algorithm we made a measurement using polymer microspheres of known calibrated size distributions.

4.3.1 *Speed*

4.3.2 *Clogging*

4.4 Optics

Using a high power LED instead of laser reduces the interference effects used in e.g. holography [20], but since it is a monochromatic source, interference may not be completely ruled out. The coherence

Chapter 4. Discussion

length, provided a Gaussian spectrum, can be approximated by Eq. 12 [1]: *equation12l*

LEDs can sometimes be used with currents far above the specifications, as long as the pulse length is short and the duty cycle is low enough to permit the heat generated to be transported away between the pulses. Using the LED above specifications may though affect the efficiency and aging of the LED. LED emittance also depends on the temperature. Depending on the capacitance of the diode, the rise time may limit the current, although there exist some techniques to shorten the LED pulses [47, 49].

The LED used was fully functional after four months of continuous measurements using 12 times higher current than specified. At 12 ampere driving current, the flash duration could be lowered to approximately 250 ns, still using the normal settings of amplification in the camera. Using even higher current would lower the flash duration still.

4.5 Droplets and Ice Interference

Droplets that are very close are likely to coalesce, thereby decreasing the number concentration at a rate that appears to increase for larger droplets and more complex droplet size distributions (Bordás, Hagemeier, Wunderlich, & Thévenin, 2011).

Due to the small depth of the measurement volume, i.e. the measuring range compared with the field of view, the likelihood of finding two droplets very close in the image is very low due to the low number concentration of droplets we are measuring.

A solution is to make a measurement of the droplet's circularity and add this as selection criteria for the measurement. This solution also works as a filter for ice or snow particles.

4.6 Icing

the risk of icing increases with increasing wind speed (Lasse Makkonen, 2000)

Calibration of true droplet size and measuring range both depends on the measured size of the droplet shadow and the amount of light

used for exposure. It is possible to predict both the precision of the measured size and accuracy for measurement of droplet size.

A value of both MVD and LWC can be derived from a series of images and since the number of measured droplets will depend on the concentration, the accuracy and precision will depend on the number of samples from the total population of droplets.

Many existing instruments suffer from errors caused by the instrument itself during sampling, e.g. when droplets get stuck on the inlet [19], or shatters into smaller droplets [20]. An instrument should be designed in order to affect the free flow of particles as little as possible [16]. Therefore we also investigate the illuminative power required to get a good exposure with the tested system at a targeted maximum wind speed of 50 m/s.

We used a stage micrometer scale for characterization of the system and simulation of water droplets. This characterization holds true given that the optical silhouette of a droplet is comparable to a dot having equal diameter and being printed on a silicon glass. It is not a new concept and has at least once been proved experimentally for coherent light, by comparing with beads of glass and water droplets of known sizes [21]. The shadow image of water drops of any size will be defined mainly by the diffracted component, as long as the distance between the drop and the lens is much larger than the drop diameter. Only in a small bright spot in the middle will the refracted component be large enough to be visible. [21, 22]. Using the results of this study, a weather protected prototype may be built to perform a comparative study. We believe that this study of a shadowgraph imaging system provides good analysis of its expected major limitations related to the measurement of liquid water content of air. This is also the scientific contribution of this publication.

The design using a weakly collimated LED that illuminates an area slightly larger than the field of view makes the system quite insensitive to misalignment of the camera and the light source. Temporal or permanent changes in light intensity caused by a minor misalignment can be automatically compensated for by continuous measurement of the total exposure level. If the level of exposure is increasing or decreasing, the length of the light pulse is changed correspondingly. The light intensity can also be affected by dirt on the front glass of

Chapter 4. Discussion

the housings.

Spatial dissimilarities in the light intensity that are not caused by noise we can compensate for by calculating the local average intensity of the background around each measured droplet. The size of a droplet is then based on the intensity dip caused by the shadow compared with its local background.

making a flat-field correction. This is done by constructing an average image by the last 20 images and using this as a

— Chapter 5 —

CONCLUSION AND OUTLOOK

5.1 Conclusions

The work shows that shadowgraph imaging can be used for precise measurements of the LWC and the MVD. Edge detection can be used to find droplets in an image and the measurement volume can be defined from a measure of the edge gradient.

The used LED is capable of emitting at much higher currents than the specified max.

The DII was proven to withstand and function in a very humid environment.

The LWC in a fog chamber can be controlled by regulating the fan speed and the power of an ultrasonic humidifier.

The resulting LWC and MVD measured by the DII can be compared with the CDP using a 30 minute average. The DII measures a lower LWC

5.2 Future Work

1. A second study of real world LWC and MVD should be done using a third instrument.
2. A simultaneous measurement of ice load should be done to find out more about the relationship between MVD, LWC and ice load.
3. The DII should be improved by increasing the image processing speed. This can be done e.g. by implementing pre-processing algorithms in hardware or by switching to a more powerful processing computer.

Chapter 5. Conclusion and Outlook

4. Higher wind speeds can be used. The LED flash can be shortened by using higher. This means changing the hardware that drives the LED to achieve a higher current.

A study to further investigate the relation between the different parameters impact on the ice load may be done using the instruments an ice monitoring device. This should be done in combination with a third independent LWC and MVD measurement, e.g. by using rotating cylinders[34].

5.3 Contributions

Paper I Paper II Paper III Paper IV

BIBLIOGRAPHY

- [1] Ceyhun Akcay, Pascale Parrein, and Jannick P Rolland. "Estimation of longitudinal resolution in optical coherence imaging". In: *Applied optics* 41.25 (2002), pp. 5256–5262.
- [2] Albert Ansmann, Maren Riebesell, and Claus Weitkamp. "Measurement of atmospheric aerosol extinction profiles with a Raman lidar". In: *Optics letters* 15.13 (1990), pp. 746–748.
- [3] D. Baumgardner. "An Analysis and Comparison of 5 Water Droplet Measuring-Instruments". In: *Journal of Climate and Applied Meteorology* 22.5 (1983), pp. 891–910.
- [4] D. Baumgardner et al. "Airborne instruments to measure atmospheric aerosol particles, clouds and radiation: A cook's tour of mature and emerging technology". In: *Atmospheric Research* 102.1-2 (2011), pp. 10–29.
- [5] D Baumgardner et al. "The cloud, aerosol and precipitation spectrometer: a new instrument for cloud investigations". In: *Atmospheric research* 59 (2001), pp. 251–264.
- [6] Craig F Bohren and Donald R Huffman. *Absorption and scattering of light by small particles*. John Wiley & Sons, 2008.
- [7] John Canny. "A computational approach to edge detection". In: *Pattern Analysis and Machine Intelligence, IEEE Transactions on* 6 (1986), pp. 679–698.
- [8] Stewart G Cober, George A Isaac, and J Walter Strapp. "Characterizations of aircraft icing environments that include supercooled large drops". In: *Journal of Applied Meteorology* 40.11 (2001), pp. 1984–2002.
- [9] Ruben D Cohen. "Shattering of a liquid drop due to impact". In: *Proceedings of the Royal Society of London A: Mathematical, Physical and Engineering Sciences*. Vol. 435. The Royal Society, 1991, pp. 483–503.

Bibliography

- [10] Paul J. Connolly et al. "Calibration of the Cloud Particle Imager Probes Using Calibration Beads and Ice Crystal Analogs: The Depth of Field". In: *Journal of Atmospheric and Oceanic Technology* 24.11 (2007), pp. 1860–1879.
- [11] N Dalili, A Edrisy, and R Carriveau. "A review of surface engineering issues critical to wind turbine performance". In: *Renewable and Sustainable Energy Reviews* 13.2 (2009), pp. 428–438.
- [12] James E Dye and Darrel Baumgardner. "Evaluation of the forward scattering spectrometer probe. Part I: Electronic and optical studies". In: *Journal of Atmospheric and Oceanic Technology* 1.4 (1984), pp. 329–344.
- [13] Jordi Estevadeordal and Larry Goss. "PIV with LED: particle shadow velocimetry (PSV)". In: *43rd AIAA aerospace sciences meeting and exhibit, meeting papers*. 2005, pp. 12355–12364.
- [14] PR Field, AJ Heymsfield, and A Bansemer. "Shattering and particle interarrival times measured by optical array probes in ice clouds". In: *Journal of Atmospheric and Oceanic Technology* 23.10 (2006), pp. 1357–1371.
- [15] S Fikke et al. "COST 727: Atmospheric Icing on structures". In: *Measurements and data collection on icing: State of the Art, Publication of MeteoSwiss* 75.110 (2006), pp. 1422–1381.
- [16] Karen J Finstad, Edward P Lozowski, and Lasse Makkonen. "On the median volume diameter approximation for droplet collision efficiency". In: *Journal of the atmospheric sciences* 45.24 (1988), pp. 4008–4012.
- [17] Rafael C Gonzales and Richard E Woods. *Digital Image Processing, 2-nd Edition*. 2002.
- [18] Gösta H Granlund. "Fourier preprocessing for hand print character recognition". In: *IEEE transactions on computers* 100.2 (1972), pp. 195–201.
- [19] George M Hale and Marvin R Querry. "Optical constants of water in the 200-nm to 200- μm wavelength region". In: *Applied optics* 12.3 (1973), pp. 555–563.

- [20] J Henneberger et al. "HOLIMO II: a digital holographic instrument for ground-based in situ observations of microphysical properties of mixed-phase clouds". In: *Atmospheric Measurement Techniques* 6.11 (2013), pp. 2975–2987.
- [21] Matthew C. Homola, Per J. Nicklasson, and Per A. Sundsbø. "Ice sensors for wind turbines". In: *Cold Regions Science and Technology* 46.2 (2006), pp. 125–131.
- [22] Matthew C. Homola et al. "Effect of atmospheric temperature and droplet size variation on ice accretion of wind turbine blades". In: *Journal of Wind Engineering and Industrial Aerodynamics* 98.12 (2010), pp. 724–729.
- [23] Matthew C Homola et al. "Performance losses due to ice accretion for a 5 MW wind turbine". In: *Wind Energy* 15.3 (2012), pp. 379–389.
- [24] Robert F Ide. *Comparison of Liquid Water Content Measurement Techniques in an Icing Wind Tunnel*. Tech. rep. DTIC Document, 1999.
- [25] William J Jasinski et al. "Wind turbine performance under icing conditions". In: *Journal of Solar Energy Engineering* 120.1 (1998), pp. 60–65.
- [26] Robert G Knollenberg. "The optical array: An alternative to scattering or extinction for airborne particle size determination". In: *Journal of Applied Meteorology* 9.1 (1970), pp. 86–103.
- [27] AV Korolev, JW Strapp, and GA Isaac. "Evaluation of the accuracy of PMS optical array probes". In: *Journal of Atmospheric and Oceanic Technology* 15.3 (1998), pp. 708–720.
- [28] AV Korolev et al. "Evaluation of measurements of particle size and sample area from optical array probes". In: *Journal of Atmospheric and Oceanic Technology* 8.4 (1991), pp. 514–522.
- [29] Linhong Kou, Daniel Labrie, and Petr Chylek. "Refractive indices of water and ice in the 0.65-to 2.5- μm spectral range". In: *Applied optics* 32.19 (1993), pp. 3531–3540.

Bibliography

- [30] Bjørn Egil Kringlebotn Nygaard, Jón Egill Kristjánsson, and Lasse Makkonen. "Prediction of In-Cloud Icing Conditions at Ground Level Using the WRF Model". In: *Journal of Applied Meteorology and Climatology* 50.12 (2011), pp. 2445–2459.
- [31] Thomas Kuhn, Igor Grishin, and JJ Sloan. "Improved imaging and image analysis system for application to measurement of small ice crystals". In: *Journal of Atmospheric and Oceanic Technology* 29.12 (2012), pp. 1811–1824.
- [32] Pramod Kulkarni, Paul A Baron, and Klaus Willeke. *Aerosol measurement: principles, techniques, and applications*. John Wiley & Sons, 2011.
- [33] RP Lawson and RH Cormack. "Theoretical design and preliminary tests of two new particle spectrometers for cloud microphysics research". In: *Atmospheric research* 35.2 (1995), pp. 315–348.
- [34] L. Makkonen. "Analysis of Rotating Multicylinder Data in Measuring Cloud-Droplet Size and Liquid Water-Content". In: *Journal of Atmospheric and Oceanic Technology* 9.3 (1992), pp. 258–263.
- [35] Lasse Makkonen. "Models for the growth of rime, glaze, icicles and wet snow on structures". In: *Philosophical Transactions of the Royal Society of London A: Mathematical, Physical and Engineering Sciences* 358.1776 (2000), pp. 2913–2939.
- [36] Lasse Makkonen et al. "Modelling and prevention of ice accretion on wind turbines". In: *Wind Engineering* 25.1 (2001), pp. 3–21.
- [37] David Marr and Ellen Hildreth. "Theory of edge detection". In: *Proceedings of the Royal Society of London. Series B. Biological Sciences* 207.1167 (1980), pp. 187–217.
- [38] Gustav Mie. "Beiträge zur Optik trüber Medien, speziell kolloidaler Metallösungen". In: *Annalen der physik* 330.3 (1908), pp. 377–445.

- [39] B. E. K. Nygaard, J. E. Kristjansson, and L. Makkonen. "Prediction of In-Cloud Icing Conditions at Ground Level Using the WRF Model". In: *Journal of Applied Meteorology and Climatology* 50.12 (2011), pp. 2445–2459.
- [40] International Standardization Organization. *ISO 12181-1: 2011, Geometrical Product Specifications (GPS)-Roundness-Part 1: Vocabulary and parameters of roundness*. 2011.
- [41] Olivier Parent and Adrian Ilinca. "Anti-icing and de-icing techniques for wind turbines: Critical review". In: *Cold regions science and technology* 65.1 (2011), pp. 88–96.
- [42] T Reisinger et al. "On the relative intensity of Poisson's spot". In: *New Journal of Physics* 19.3 (2017), p. 033022.
- [43] Staffan Rydholm and Benny Thornberg. "Liquid Water Content and Droplet Sizing Shadowgraph Measuring System for Wind Turbine Icing Detection". In: *IEEE Sensors Journal* 16.8 (2015), pp. 2714–2725.
- [44] Wayne R Sand et al. "Icing conditions encountered by a research aircraft". In: *Journal of climate and applied meteorology* 23.10 (1984), pp. 1427–1440.
- [45] Jaiwon Shin and Thomas H Bond. *Results of an icing test on a NACA 0012 airfoil in the NASA Lewis Icing Research Tunnel*. National Aeronautics and Space Administration, 1992.
- [46] J. K. Spiegel et al. "Evaluating the capabilities and uncertainties of droplet measurements for the fog droplet spectrometer (FM-100)". In: *Atmospheric Measurement Techniques* 5.9 (2012), pp. 2237–2260.
- [47] Hiroyuki Tanaka, Yohtaro Umeda, and Osamu Takyu. "High-speed LED driver for visible light communications with drawing-out of remaining carrier". In: *Radio and Wireless Symposium (RWS), 2011 IEEE*. IEEE, 2011, pp. 295–298.
- [48] Gregory Thompson et al. "Using the Weather Research and Forecasting (WRF) model to predict ground/structural icing". In: *13th International Workshop on Atmospheric Icing on Structures, METEOTEST, Andermatt, Switzerland*. 2009.

Bibliography

- [49] Omar Veledar et al. "Simple techniques for generating nanosecond blue light pulses from light emitting diodes". In: *Measurement Science and Technology* 18.1 (2007), p. 131.
- [50] Timothy P Wallace and Paul A Wintz. "An efficient three-dimensional aircraft recognition algorithm using normalized Fourier descriptors". In: *Computer Graphics and Image Processing* 13.2 (1980), pp. 99–126.
- [51] AD Ward, M Zhang, and O Hunt. "Broadband Mie scattering from optically levitated aerosol droplets using a white LED". In: *Optics express* 16.21 (2008), pp. 16390–16403.
- [52] Manfred Wendisch and Jean-Louis Brenguier. *Airborne measurements for environmental research : methods and instruments*. Wiley Series in Atmospheric Physics and Remote Sensing. Weinheim: Wiley-VCH, 2013.
- [53] CD Westbrook et al. "Estimating drizzle drop size and precipitation rate using two-colour lidar measurements". In: *Atmospheric Measurement Techniques* 3.3 (2010), pp. 671–681.
- [54] C. Willert et al. "Pulsed operation of high-power light emitting diodes for imaging flow velocimetry". In: *Measurement Science and Technology* 21.7 (2010), p. 075402.